5-20-2001

Supernumerary Spacing of Rainbows Produced by an Elliptical-Cross-Section Cylinder. II. Experiment

Charles L. Adler

David Phipps

Kirk W. Saunders

Justin K. Nash

James A. Lock
Cleveland State University, j.lock@csuohio.edu

Publisher's Statement

Original Citation

Adler, Charles L., David Phipps, Kirk W. Saunders, Justin K. Nash, and James A. Lock. "Supernumerary Spacing of Rainbows Produced by an Elliptical-Cross-Section Cylinder. II. Experiment." *Applied Optics* 40 (2001): 2535-2545.

Supernumerary spacing of rainbows produced by an elliptical-cross-section cylinder. II. Experiment

Charles L. Adler, David Phipps, Kirk W. Saunders, Justin K. Nash, and James A. Lock

We measured the supernumerary spacing parameter of the first- and second-order rainbows of two glass rods, each having an approximately elliptical cross section, as a function of the rod's rotation angle. We attribute large fluctuations in the supernumerary spacing parameter to small local inhomogeneities in the rod's refractive index. The low-pass filtered first-order rainbow experimental data agree with the prediction of ray-tracing–wave-front modeling to within a few percent, and the second-order rainbow data exhibit additional effects that are due to rod nonellipticity. © 2001 Optical Society of America

OCIS codes: 290.0290, 290.3030, 290.5820, 080.1510.

1. Introduction

When a beam of light is scattered by a homogeneous cylinder whose cross section is circular or nearly so, a series of rainbows occur in the scattered intensity, each corresponding to a different number of internal reflections of the light before exiting the cylinder. Each rainbow is flanked on one side by a supernumerary interference pattern, caused by the alternating constructive and destructive interference of rays incident on the cylinder to either side of the rainbow ray. When the incident beam is normal to the axis of a cylinder having a circular cross section, each rainbow remains unchanged as the cylinder is rotated about its axis. But if the cylinder's cross section is elliptical, the rainbow angle, the intensity of the rainbow, and the spacing of the supernumerary maxima oscillate about their respective circular cross-sectional values as the cylinder is rotated about its axis. For a slightly elliptical cylinder, the oscillation of the first-order rainbow angle was calculated in 1909 by Möbius[1,2] who truncated the equations for ray propagation inside the cylinder at first order in the cylinder ellipticity. More recently, the Möbius calculation was extended to the second-order rainbow angle,[3] and the effect that the ellipticity of falling raindrops has on the supernumeraries of the first-order rainbow in rain showers[4,5] and the observed absence of supernumeraries of the second-order rainbow[3] were investigated.

In Ref. 6 we theoretically examined the dependence of the supernumerary spacing parameter h of the first-order rainbow of an elliptical cross-sectional cylinder on the cylinder's rotation angle ξ. We numerically traced a collection of closely spaced rays in the vicinity of the rainbow ray through the cylinder and computed the optical path length of the rays with respect to that of the rainbow ray. We fitted the phase front of the rays exiting the cylinder to a fourth-degree polynomial and identified the coefficient of the cubic term with the supernumerary spacing parameter.[7] Based on our numerical results, we obtained an approximate expression for $h(\xi)$ for the first-order rainbow.

In this paper we compare the ray-tracing–wave-front modeling prediction with the experimentally measured supernumerary spacing parameter of the first- and second-order rainbows for two near-optical quality glass rods, each of which has a nearly elliptical cross section. The principal result of Ref. 6 was that h is a remarkably delicate feature of the rainbow caustic, and its accurate determination requires that the relative position of a number of supernumerary maxima be measured with great accuracy. Similarly, our principal result here is that, although small local inhomogeneities in the rod's refractive index affect the rainbow angle only negligibly, the supernumerary spacing parameter appears to be surprisingly sensitive to them. We can compensate for this

C. L. Adler, D. Phipps, K. W. Saunders, and J. K. Nash are with the Department of Physics, St. Mary's College of Maryland, St. Mary's City, Maryland 20686. J. A. Lock (jimandcarol@stratos.net) is with the Department of Physics, Cleveland State University, Cleveland, Ohio 44115.

Received 14 July 2000; revised manuscript received 4 January 2001.

0003-6935/01/152535-11$15.00/0

sensitivity by measuring $h(\xi)$ at small intervals of $\Delta\xi$ and low-pass filtering the result.

This paper is organized as follows. In Section 2 we briefly review the dependence of the first-order rainbow angle ${\theta_2}^R$ and supernumerary spacing parameter h_2 of an elliptical cross-sectional cylinder on the angle ξ that the incident plane-wave's propagation direction makes with the major axis of the cross section. We then determine both the effect that the ξ dependence of h_2 has on the measurement of the rainbow angle and the effect that the precision of the measurement of the angular position of the supernumerary maxima has on h_2. In Section 3.A we determine $h_2(\xi)$ for the rainbow data of one of the cylinders examined by Möbius, and in Sections 3.B and 3.C we determine $h_2(\xi)$ for two larger glass rods examined in our laboratory. Based on the close agreement between the low-pass filtered experimental data and the ray-tracing–wave-front modeling predictions, in Section 3.D we determine $h_3(\xi)$ for the second-order rainbow for the two glass rods and compare the results with the theoretical prediction. Finally, in Section 4 we discuss the relevance of these results to the nonintrusive flow diagnostic technique of rainbow refractometry.

2. Measurement of the Supernumerary Spacing Parameter

Consider an electromagnetic plane wave of wavelength λ normally incident on a homogeneous circular cylinder of refractive index n, radius a, and size parameter

$$x = 2\pi a/\lambda. \tag{1}$$

When x is of the order of a few thousand or more, the scattered intensity in the vicinity of the p rainbow is approximated quantitatively by Airy theory[7–9]:

$$I(\theta) \propto \mathrm{Ai}^2[-x^{2/3}(\theta - {\theta_p}^c)/({h_p}^c)^{1/3}], \tag{2}$$

where $p = 2$ denotes the first-order rainbow, $p = 3$ denotes the second-order rainbow, etc., and Ai is the Airy integral.[10] The Descartes angle of the p rainbow ${\theta_p}^c$ of a circular cross-sectional cylinder (denoted by the superscript c) in ray theory is[11]

$$\begin{aligned} \cos({\phi_i}^c) &= [(n^2 - 1)/(p^2 - 1)]^{1/2}, \\ \sin({\phi_t}^c) &= (1/n)\sin({\phi_i}^c), \\ {\theta_p}^c &= (p - 1)\pi + 2{\phi_i}^c - 2p{\phi_t}^c, \end{aligned} \tag{3}$$

where ${\phi_i}^c$ and ${\phi_t}^c$ are the angle of incidence and refraction of the Descartes rainbow ray at the cylinder surface. The supernumerary spacing parameter ${h_p}^c$ is[8]

$${h_p}^c = [(p^2 - 1)^2(p^2 - n^2)^{1/2}]/[p^2(n^2 - 1)^{3/2}]. \tag{4}$$

The region of quantitative validity of Airy theory for the $p = 2$ rainbow extends[8,9] approximately 2° to either side of ${\theta_2}^c$. For $n \approx 1.5$, this corresponds approximately to

$$N \approx 0.02x^{2/3} \tag{5}$$

supernumerary fringes.

Because the rainbow is a structurally stable caustic, its basic morphology does not change under small perturbations of the cylinder shape.[12] Thus for an elliptical cross-sectional cylinder with semimajor and semiminor axes b and a and eccentricity

$$\epsilon = (b/a) - 1, \tag{6}$$

the various features of the rainbow become functions of the cylinder's rotation angle ξ. The scattered intensity in the vicinity of the p rainbow is approximately[6]

$$I(\theta, \xi) \propto \mathrm{Ai}^2\{-{x_{\mathrm{ave}}}^{2/3}[\theta - {\theta_p}^R(\xi)]/{h_p}(\xi)^{1/3}\}, \tag{7}$$

where x_{ave} is the average cylinder size parameter. If the cylinder size parameter is in the geometrical-optics regime and ϵ is less than a few percent, the $p = 2$ rainbow angle is approximated accurately by the ray theory result of Möbius[1,2]:

$${\theta_2}^R(\xi) = {\theta_2}^c - \Delta{\theta_2}^R \cos(2\xi + {\theta_2}^c) + O(\epsilon^2), \tag{8}$$

where

$$\Delta{\theta_2}^R = 8\epsilon \sin({\phi_t}^c)\cos^3({\phi_t}^c) \tag{9}$$

is the amplitude of oscillation of the rainbow angle. Similarly, in Ref. 6 we found that the supernumerary spacing parameter of the $p = 2$ rainbow is approximated accurately in the geometrical-optics regime for small ϵ and $1.25 \le n \le 1.7$ by

$$h_2(\xi) \approx {h_2}^c + \Delta h_2 \cos(2\xi + \Phi_2), \tag{10}$$

where

$$\Delta h_2 \approx 19\epsilon[\sin({\phi_t}^c)]^{3/4}[\cos({\phi_t}^c)]^{-10/3} \tag{11}$$

is the amplitude of oscillation of the supernumerary spacing parameter and

$$\Phi_2 \approx (250°)n - 285° \tag{12}$$

is the phase of the oscillation.

Experimentally, we can obtain the $p = 2$ rainbow angle as a function of ξ for an elliptical cross-sectional cylinder by measuring the angle of the first supernumerary maximum ${\theta_a}^{\max}(\xi)$ in degrees and by using the Airy theory result of relation (7),

$$\begin{aligned} 1.018\ 793 = (\pi/180){x_{\mathrm{ave}}}^{2/3}[{\theta_a}^{\max}(\xi) \\ - {\theta_2}^R(\xi)]/[h_2(\xi)]^{1/3}, \end{aligned} \tag{13}$$

to obtain

$$\begin{aligned} {\theta_2}^R(\xi) = {\theta_a}^{\max}(\xi) - 1.018\ 793\ (180/\pi) \\ \times [h_2(\xi)]^{1/3}/({x_{\mathrm{ave}}})^{2/3}, \end{aligned} \tag{14}$$

where Ai(−1.018 793) is the first relative maximum of the Airy integral.[10] In practice, the ξ dependence of h_2 is ignored,[13] and $\theta_2{}^R(\xi)$ is obtained by

$$\theta_2{}^R(\xi) \approx \theta_a{}^{\max}(\xi) - 1.018\ 793\ (180/\pi) \times (h_2{}^c)^{1/3}/(x_{\text{ave}})^{2/3}. \tag{15}$$

The replacement of $h_2(\xi)$ for an elliptical cross-sectional cylinder by $h_2{}^c$ for a circular cross-sectional cylinder in approximation (15) is of no practical consequence in the measurement of the rainbow angle in the geometrical-optics regime, e.g., $x \gtrsim 10^4$, when the eccentricity ϵ is small as is illustrated by the following three examples. First, in Refs. 1 and 2, Möbius reported the measurement of the position of a number of the supernumerary maxima of the $p = 2$ rainbow as a function of ξ for three glass rods and three glass spheres illuminated by a sodium lamp of $\lambda = 0.5894\ \mu$m. His rod C2 had $a = 1.0$ mm, $n = 1.511$, and size parameter $x \approx 10{,}600$. With $\epsilon \approx 0.00155$, it had the largest eccentricity of any of the six samples. Thus, according to approximation (11), it should have had the largest and most easily observable oscillation of $h_2(\xi)$. The $p = 2$ supernumerary spacing parameter of Eq. (4) for a circular cross-sectional cylinder with $n = 1.511$ is $h_2{}^c = 2.028$; and for an elliptical cross section with $\epsilon \approx 0.00155$, the amplitudes of the oscillation of $\theta_2{}^R(\xi)$ and $h_2(\xi)$ in Eq. (9) and approximation (11) are $\Delta\theta_2{}^R \approx 0.231°$ and $\Delta h_2 \approx 0.028$. Substitution of the range of h values $2.000 \leq h_2 \leq 2.056$ into Eq. (14) causes an uncertainty in $\Delta\theta_2{}^R$ of only 0.31%. Second, in our previous experiments[13–16] on the $p = 2$ and $p = 3$ rainbows of a glass rod with $a = 8.05$ mm, $n = 1.474$, and $x \approx 80{,}000$ illuminated by $\lambda = 0.6328$-μm He–Ne laser light, the rod's cross section was found to be nearly elliptical with $\epsilon \approx -0.037$. Equation (4) for a circular cross-sectional cylinder with $n = 1.474$ yields $h_2{}^c = 2.395$; and for an elliptical cross section with $\epsilon \approx -0.037$, the amplitudes of the oscillation of $\theta_2{}^R(\xi)$ and $h_2\ (\xi)$ are $\Delta\theta_2{}^R \approx 5.48°$ and $\Delta h_2 \approx 0.755$. The ξ dependence of h_2 causes an uncertainty in $\Delta\theta_2{}^R$ of only 0.08%. Third, in Section 3 we also report measurements made in our laboratory on the $p = 2$ and $p = 3$ rainbows of another glass rod with $a = 2.44$ mm, $n = 1.502$, and $x \approx 24{,}000$ illuminated by $\lambda = 0.6328$-μm He–Ne laser light. The rod's cross section is nearly elliptical with $\epsilon \approx 0.0054$. Equation (4) for a circular cross-sectional cylinder with $n = 1.502$ yields $h_2{}^c = 2.111$; and for $\epsilon \approx 0.0054$, the amplitude of the oscillation of $\theta_2{}^R(\xi)$ and $h_2(\xi)$ is $\Delta\theta_2{}^R \approx 0.80°$ and $\Delta h_2 \approx 0.101$. The ξ dependence of h_2 causes an uncertainty in $\Delta\theta_2{}^R$ of only 0.18%.

Experimentally, both the $p = 2$ rainbow angle and the supernumerary spacing parameter can be obtained as a function of ξ when we measure the angle of the first and second supernumerary maxima $\theta_a{}^{\max}(\xi)$ and $\theta_b{}^{\max}(\xi)$ in degrees and use the Airy theory result of relation (7),

$$\begin{aligned} 1.018\ 793 &= (\pi/180)(x_{\text{ave}})^{2/3}[\theta_a{}^{\max}(\xi) - \theta_2{}^R(\xi)]/[h_2(\xi)]^{1/3}, \\ 3.248\ 198 &= (\pi/180)(x_{\text{ave}})^{2/3}[\theta_b{}^{\max}(\xi) - \theta_2{}^R(\xi)]/[h_2(\xi)]^{1/3}, \end{aligned} \tag{16}$$

to obtain

$$\theta_2{}^R(\xi) = (1.456\ 980)\theta_a{}^{\max}(\xi) - (0.456\ 980)\theta_b{}^{\max}(\xi), \tag{17}$$

$$h_2(\xi) = (0.479\ 806)(10^{-6})(x_{\text{ave}})^2[\theta_b{}^{\max}(\xi) - \theta_a{}^{\max}(\xi)]^3, \tag{18}$$

where Ai(−3.248 198) is the first relative minimum of the Airy integral.[10] If $\delta\theta_{ab}$ is the uncertainty in the measured angle of each of the two supernumerary maxima in degrees, the resulting uncertainty in $\theta_2{}^R(\xi)$ and $h_2(\xi)$ is obtained when we differentiate Eqs. (17) and (18), yielding

$$(\delta\theta_2{}^R)_{\text{measured}} \approx \delta\theta_{ab}, \tag{19}$$

$$(\delta h_2)_{\text{measured}} \approx (0.02349)\delta\theta_{ab}(x_{\text{ave}}h_2{}^c)^{2/3}. \tag{20}$$

In the complex angular momentum approximation to Mie theory, a number of corrections to Airy theory are derived for a spherical particle or a circular cross-sectional cylinder.[17] These include a progressive stretching of the supernumerary interference pattern with respect to the predictions of Airy theory, which introduces small corrections to Eqs. (16). These corrections were addressed in Ref. 6 and were found to improve the agreement between Mie theory and the complex angular momentum-corrected version of Eqs. (16) for rainbows produced by a circular cross-sectional cylinder. The complex angular momentum circular cross-sectional corrections applied to the first few supernumerary maxima for an elliptical cross-sectional cylinder, however, did not improve the agreement and thus are not pursued further here.

We now demonstrate, using the three examples considered in the previous paragraph, that the $p = 2$ rainbow angle is not especially sensitive to the precision of the measurement of the two supernumerary maxima. But an accurate determination of $h_2(\xi)$ requires that the two supernumerary maxima be measured with great precision. For the Möbius measurements of the rod C2, the supernumerary angle accuracy was $\delta\theta_{ab} = 2.78 \times 10^{-4}$ deg, yielding $(\delta\theta_2{}^R)_{\text{measured}} = 1.2 \times 10^{-3}\ (\Delta\theta_2{}^R)$. Thus the oscillation in the rainbow angle should be resolvable to approximately 0.1%. Rather than using the first and second supernumerary maxima, Möbius measured the relative position of the second and tenth intensity maxima. When the quantitative validity of Airy theory is assumed out to the tenth supernumerary for a rod of this size [see approximation (5)], approximation (20) yields $(\delta h_2)_{\text{measured}} = 0.04(\Delta h_2)$.

Again, the oscillation in the supernumerary spacing parameter should be resolvable to approximately 4%. In a comparison of the ratio $(\delta h_2)_{\text{measured}}/(\Delta h_2)$ with $(\delta\theta_2{}^R)_{\text{measured}}/(\Delta\theta_2{}^R)$, the measured uncertainty in h_2 is approximately 36 times greater than the measured uncertainty in $\theta_2{}^R$. Similarly, in the experiment described in Subsection 3.B for the 8.05-mm-radius glass rod, we measured the position of the first and second supernumerary maxima of the $p = 2$ rainbow using a CCD camera with pixels of width 9.61 ± 0.32 μm located $r = 341$ mm from the rod's axis. The supernumerary maxima are determined with an accuracy of ± 1.5 pixels, or $\delta\theta_{ab} = 2.4 \times 10^{-3}$ deg, which yields $(\delta\theta_{ab})_{\text{measured}} = 4.4 \times 10^{-4}$ $(\Delta\theta_2{}^R)$ and $(\delta h_2)_{\text{measured}} = 0.25\,(\Delta h_2)$. Again, when we compare the ratios, the uncertainty in the measured value of h_2 is approximately 570 times greater than the measured uncertainty in $\theta_2{}^R$. The measurement uncertainty in $h_2(\xi)$ should be substantial in this case, but the oscillation of amplitude Δh_2 should certainly be observable. Finally, for the experiment described in Subsection 3.C on the 2.44-mm-radius glass rod, the CCD array was $r = 132$ mm from the rod's axis yielding $\delta\theta_{ab} = 6.3 \times 10^{-3}$ deg, $(\delta\theta_{ab})_{\text{measured}} = 7.8 \times 10^{-3}(\Delta\theta_2{}^R)$, and $(\delta h_2)_{\text{measured}} = 2.01(\Delta h_2)$. The uncertainty in the measured value of h_2 is approximately 260 times greater than the measured uncertainty in $\theta_2{}^R$.

Because the measurement uncertainty in h_2 for the second glass rod is twice the amplitude of oscillation of $h_2(\xi)$, we would not expect the oscillation to be resolvable unless some type of averaging procedure were used. For example, if the first and third, or the first and fourth, supernumerary maxima were measured with a precision of $\pm\delta\theta_{ab}$ deg and Airy theory was presumed to be quantitatively accurate to the fourth supernumerary for the size parameter of the second rod [see approximation (5)], the resulting uncertainty in h_2 falls to $(\delta h_2)_{\text{measured}} = 1.17(\Delta h_2)$ and $(\delta h_2)_{\text{measured}} = 0.88(\Delta h_2)$, respectively. By measuring the positions of the supernumerary maxima using a small $\Delta\xi$ interval, averaging the results obtained from a number of pairs of supernumeraries, and then low-pass filtering the average as a function of ξ, we would sufficiently decrease the uncertainty noise so as to resolve the oscillation in $h_2(\xi)$ experimentally for this case.

3. Experimental Determination of $h_2(\xi)$

A. Möbius Sample C2

For the glass rod C2, Möbius measured the position of the second and tenth supernumerary maxima of the $p = 2$ rainbow at intervals of $\Delta\xi = 22.5°$. His results are given in Table 12 of Ref. 1 and Table 10 of Ref. 2. Analyzing these data with Eqs. (17) and (18) modified to the second and tenth supernumerary maxima, corresponding to Ai(−3.248 198) and Ai(−12.384 788), we determined $\theta_2{}^R(\xi)$ and $h_2(\xi)$, which are shown as the solid circles in Figs. 1(a) and 1(b), respectively. The experimental data yield $\Delta\theta_2{}^R \approx 0.231°$ and $(h_2)_{\text{ave}} \approx 2.0274$ averaged over the 17 values of ξ.

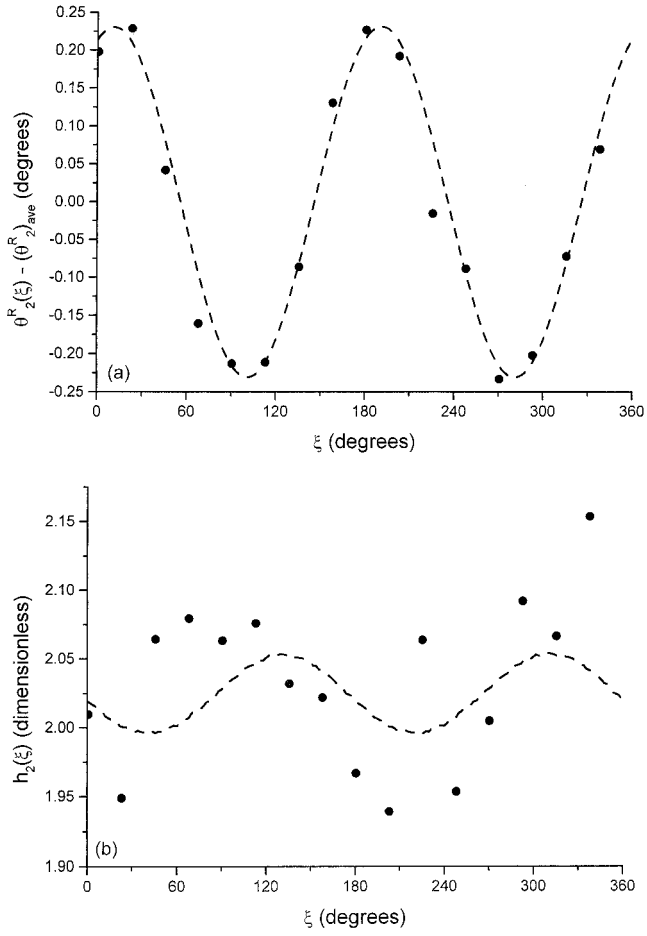

Fig. 1. (a) Deviation of the $p = 2$ rainbow angle from its average value and (b) supernumerary spacing parameter of a 1.0-mm-radius glass rod with refractive index $n = 1.511$ and eccentricity $\epsilon = 0.00155$ as a function of the rod's rotation angle. The solid circles are the experimental data of Ref. 1, and the dashed curves are the predictions of the ray-tracing–wave-front modeling procedure of Ref. 6.

Möbius measured the eccentricity of rod C2 to be $\epsilon = 0.001$ using a micrometer to test the validity of Eqs. (8) and (9). We previously found,[13] however, that assuming the correctness of Eqs. (8) and (9) and fitting the observed oscillation of $\theta_2{}^R(\xi)$ to the equations yields a much more accurate estimate of the eccentricity. The dashed curve in Fig. 1(a), corresponding to an eccentricity of $\epsilon = 0.00155$ obtained from Eqs. (8) and (9), matches the $p = 2$ rainbow position data quite nicely.

We analyzed the experimental results for the supernumerary spacing parameter of Fig. 1(b) as follows. First we computed $h_2(\xi)$ for $n = 1.511$ and $\epsilon = 0.00155$ using the ray-tracing–wave-front modeling procedure of Ref. 6. The results are shown as the dashed curve in Fig. 1(b). We then performed the Fourier-series decomposition of the ray-tracing–wave-front modeling result,

$$h_2(\xi) = e_0 + \sum_{m=1}^{\infty} e_m \cos(m\xi) + \sum_{m=1}^{\infty} f_m \sin(m\xi), \quad (21)$$

and compared the average of the experimental results with the $m = 0$ theoretical Fourier coefficient. The theoretical $m = 0$ Fourier coefficient was 2.0243, which differs from the experimental $(h_2)_{\text{ave}}$ by only 0.15%.

The ξ dependence of the experimental data for $h_2(\xi)$ in Fig. 1(b), however, only vaguely resembles the ray-tracing–wave-front modeling prediction. The data possess a surprisingly high noise level. The root-mean-square deviation of the experimental data of Fig. 1(b) from $(h_2)_{\text{ave}}$ is 182% of the value of $\Delta h_2(\xi)$ predicted from approximation (11). This is surprising because our estimate of the measurement uncertainty in Section 2 was approximately only 4% of $\Delta h_2(\xi)$. We also compared the experimental results for Möbius's other spheres and cylinders to the ray-tracing–wave-front modeling predictions and found the comparison to be considerably poorer than for the sample C2 rod. This is because the eccentricity, and thus the expected oscillation in $h_2(\xi)$, is much smaller for the other samples.

We conjecture that the large noise level in the experimental data of Möbius is due to perturbations in the shape of the wave front exiting the rod caused by small localized inhomogeneities in the rod's refractive index or small imperfections in the rod. We call this effect inhomogeneity noise and discuss it more in Subsection 3.B. The interval of the rod rotation angle used by Möbius, $\Delta\xi = 22.5°$, is too coarse to perform low-pass filtering on the data to determine whether the expected oscillation in h_2 is present beneath the inhomogeneity noise.

B. $p = 2$ Supernumeraries of the 8.05-mm-Radius Glass Rod

We also encountered an unexpectedly high amount of inhomogeneity noise in our experimental determination of $h_2(\xi)$. As a result, in this subsection we give a detailed description of the tests we made on our apparatus to ensure that the noise was not an artifact of the measurement procedure. First, the rationale for our choice of glass rods is as follows. Before the measurements of the $p = 2$ and $p = 3$ rainbows reported in Ref. 13 were made, we tested a number of different glass and plastic rods of different radii and eccentricities, looking for a suitable sample. Almost all the potential samples were discarded immediately because the $p = 2$ and $p = 3$ rainbows and their supernumeraries appeared as a series of wavy parallel lines, rather than as a series of straight parallel lines. This was due to the rods possessing visible striae or small bubbles or imperfections that distorted the shape of the wave front exiting the rod. Our criterion for a suitable sample was that the $p = 2$ and $p = 3$ rainbows and their supernumeraries must visually appear as parallel straight lines on the viewing screen. We believed that this criterion was sufficient to ensure that any striae or imperfections in the rod were acceptably small. The 8.05-mm-radius rod chosen for the experiments of Ref. 13, as well as for the experiments reported here, was described by the vendor[18] as a near-optical quality artist's glass. Visual inspection showed no striae or bubbles, and the $p = 2$ and $p = 3$ rainbows and their supernumeraries seen on a distant viewing screen were a series of straight parallel lines. Slight imperfections in the glass were detected only when a 10-mW He–Ne laser, expanded to a diameter of approximately 1 cm, illuminated the center of the rod. In this case the beam transmitted directly through the rod showed a small amount of brightness variation, corresponding to weak striae or local inhomogeneities. The 2.44-mm glass rod was also free of bubbles and visible striae and produced parallel straight lines for the $p = 2$ and $p = 3$ rainbows and their supernumeraries. Thus both rods were judged to be of sufficient optical quality to serve as samples for our $p = 2$ and $p = 3$ rainbow experiments.

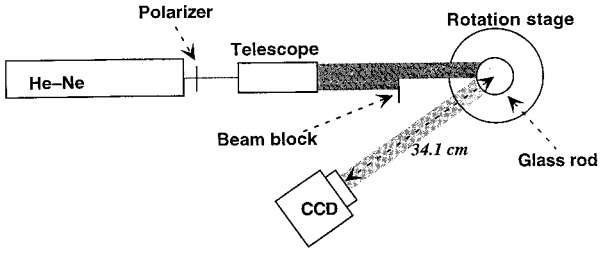

Fig. 2. Beam of a 3-mW He–Ne laser is attenuated by a polarizing filter, expanded by an afocal telescope, and is incident on a glass rod mounted on a rotation stage. A beam block prevents interference of reflected light from the rod with the $p = 2$ and $p = 3$ rainbows. The rainbow pattern is recorded by a CCD camera placed in the scattering near zone.

Our experimental apparatus for measuring the $p = 2$ and $p = 3$ rainbows of the 8.05- and 2.44-mm-radius glass rods is shown in Fig. 2. The beam from a smaller 3-mW He–Ne laser, partially polarized parallel to the rod axis, was spatially filtered and then expanded to a diameter of 2.5 cm with an afocal telescope. The expanded beam illuminated the glass rod, which was aligned to stand vertically at the center of a rotation stage. To prevent saturation of the 8-bit 640×480 pixel CCD camera that was used to record the scattered intensity in the vicinity of the rainbow, a photographic-grade polarizing filter, with its polarization direction parallel to the rod axis, was used to decrease the beam power to approximately 0.3 mW. The resulting rainbow signal on the CCD array was more than a factor of 10^2 larger than the array's dark current. The orientation of the polarizing filter was not changed during the experiment, although somewhat of a change in orientation did not change the measured supernumerary spacing. We used a razor blade as a beam block to ensure that only rays near the rainbow ray were incident on the rod. Thus there were no specularly reflected rays that otherwise would have been incident on the side of the rod opposite the rainbow ray, and which would have caused a fine interference structure superimposed on the rainbow supernumeraries. Care was taken to ensure that diffraction from the razor blade did not optically interfere with the rainbow supernumerary

Table 1. Magnitude of the Coefficients in the Fourier-Series Decomposition of $h_2(\xi)$ for the 8.05- and 2.44-mm-Radius Glass Rods[a]

	a = 8.05 mm			a = 2.44 mm	
Fourier Coefficient	Experiment (1 + 2)	Experiment (1 + 3)	Theory	Experiment	Theory
e_0	2.593	2.566	2.592	2.191	2.175
$(e_1^2 + f_1^2)^{1/2}$	0.043	0.135	0.000	0.043	0.000
$(e_2^2 + f_2^2)^{1/2}$	0.829	0.904	0.790	0.115	0.100
$(e_3^2 + f_3^2)^{1/2}$	0.478	0.517	0.000	0.042	0.000
$(e_4^2 + f_4^2)^{1/2}$	0.287	0.413	0.126	0.040	0.002
$(e_5^2 + f_5^2)^{1/2}$	0.497	0.447	0.000	0.058	0.000
$(e_6^2 + f_6^2)^{1/2}$	0.537	0.473	0.019	0.045	2×10^{-4}

[a]Experiments (1 + 2) and (1 + 3) correspond to the measurement of the first and second and the first and third supernumerary maxima of the 8.05-mm rod, respectively. For the 2.44-mm-radius glass rod, the experimental coefficients are the result of averaging $h_2(\xi)$ obtained from the first and second, first and third, and first and fourth supernumerary maxima. The ray-tracing–wave-front modeling Fourier coefficients are for $n = 1.474$ and $\epsilon = -0.037$ and for $n = 1.511$ and $\epsilon = 0.0054$. The $m = 0$ theoretical coefficient was corrected for near-zone effects with $r/a = 42.35$ for the larger rod and $r/a = 54.14$ for the smaller rod.

pattern. To decrease the background light as much as possible, all the measurements were made in a darkened room.

The CCD camera was mounted on a rotating arm that was at the same height as the incident laser beam. The rotating arm was mounted on a pivot concentric with the glass rod, and we took care to ensure that the plane of the CCD array was parallel to the rod axis. During each measurement of either the $p = 2$ or $p = 3$ rainbow, we rotated the glass rod in increments of $\Delta\xi = 2°$, and before each measurement we adjusted the camera position so that the first supernumerary maximum was at the center of the CCD array. Because the rainbow intensity varies as a function of ξ, the supernumerary maxima-to-minima contrast varied between 45/1 at best and 10/1 at worst. The CCD array was used in a lensless configuration, and approximately 50 rows of pixels, corresponding to a height of slightly less than 1 mm on the array, were averaged to decrease statistical fluctuations. Because the rainbows and their supernumeraries visually appeared as a series of parallel straight lines and the columns of CCD pixels were aligned with the supernumerary fringes, the averaging procedure did not reduce the fringe contrast. The supernumerary intensity pattern was recorded only once for each ξ. But when many frames were recorded at a given ξ and the results were averaged, the resulting supernumerary spacing did not change.

To ensure that the diffraction pattern from the beam block was not affecting our measurements, we repeated the measurements without the beam block present. Although the overall background noise increased, the spacing of the supernumerary pattern did not change. The CCD camera initially had a thin IR filter on its active surface. We removed this to ensure that reflections inside the IR filter were not affecting the supernumerary pattern. Removal of the filter produced no change in the supernumerary structure, although it did eliminate a high-frequency ripple superimposed on it. All the measurements reported here were taken after the filter was removed.

The spacing between the first and second and the first and third supernumerary maxima was used to determine the supernumerary spacing parameter from Eq. (18), and the results were decomposed into a Fourier series as in Eq. (21). Our experimental results for $h_2(\xi)$ for the 8.05-mm-radius rod are shown in Table 1 and in Figs. 3(a) and 3(b). The column in Table 1 labeled Experiment (1 + 2) and the data in Fig. 3(a) are determined from the first and second supernumerary maxima, and the column in Table 1 labeled Experiment (1 + 3) and the data in Fig. 3(b) are determined from the first and third supernumerary maxima. In Table 1 the magnitude of the Fourier coefficients is displayed for $0 \le m \le 6$, rather than the individual coefficients themselves; and the experimental data of Figs. 3(a) and 3(b) were cyclically permuted until the phase of the experimental $m = 2$ Fourier coefficient matched that of the theoretical $m = 2$ Fourier coefficient. This was done because, at the beginning of the experimental run, we were not able to align the rod accurately with the theoretical $\xi = 0°$ orientation. This was also the case for our measurement of the $p = 2$ and $p = 3$ rainbow angle in Ref. 13.

We obtained the theoretical values of the Fourier coefficients in Table 1 using the ray-tracing–wave-front modeling procedure of Ref. 6 with $n = 1.474$ and $\epsilon = -0.037$. The odd-m theoretical coefficients vanish identically because of the 180° rotational symmetry of the cylinder cross section. The 4.2% near-zone correction of Ref. 19 for a circular cross-sectional cylinder was applied to the $m = 0$ theoretical coefficient appearing in Table 1 because the experimental measurements were made at $r/a = 42.35$ rather than infinitely far from the rod. No near-zone correction was applied to the $m \ge 2$ Fourier coefficients. In Figs. 3(a) and 3(b) the filled circles are the experimental data points, the solid curves are the low-pass filtered experimental data containing only the $0 \le m \le 4$ Fourier series terms, and the dashed curves

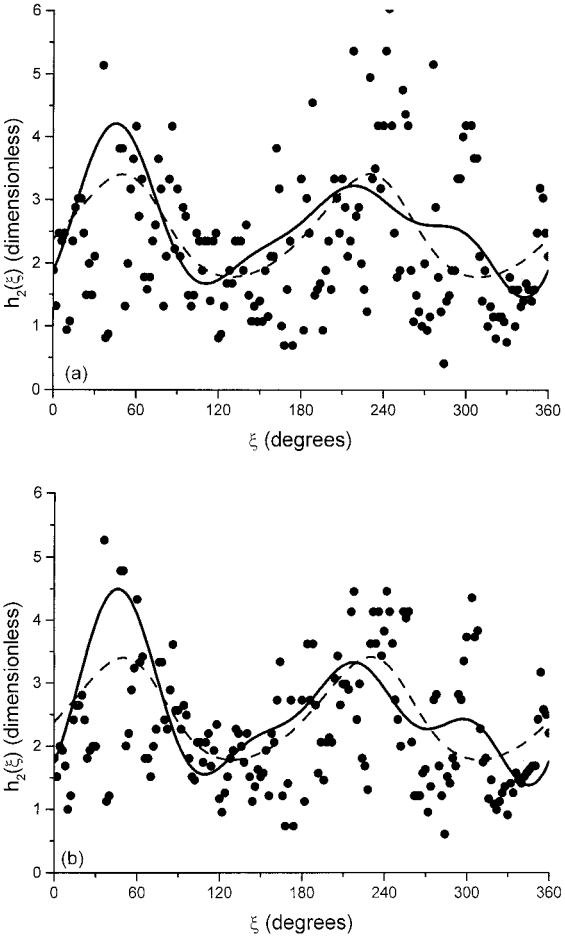

Fig. 3. Supernumerary spacing parameter of the $p = 2$ rainbow of a 8.05-mm-radius glass rod with refractive index $n = 1.474$ and eccentricity $\epsilon = -0.037$ as a function of the rod's rotation angle. The solid circles are the experimental data obtained from (a) the first and second supernumerary maxima and (b) the first and third supernumerary maxima. The solid curves are the low-pass filtered experimental data, and the dashed curves are the predictions of the ray-tracing–wave-front modeling procedure of Ref. 6.

are the ray-tracing–wave-front modeling prediction of Ref. 6. The cutoff of the low-pass filtering of the experimental data was chosen to be $m = 4$ because the theoretical Fourier coefficients of $h_2(\xi)$ in Table 1 are negligible for $m \geq 6$. It can be argued that the choice of $m = 4$ for the low-pass cutoff of the experimental data is somewhat arbitrary. If we had cut off the Fourier series at $m = 2$ or $m = 3$, the agreement between the filtered data and the theoretical prediction would have been greatly improved. But if we had used a cutoff of $m \geq 5$, the low-pass data would have exhibited some higher-frequency periodicity, and the comparison would have deteriorated somewhat. We believe that the $m = 4$ cutoff represents a realistic trade-off between these two tendencies.

The average values of h_2 in the interval $0° \leq \xi \leq 360°$ for the experimental data of Figs. 3(a) and 3(b) are $(h_2)_{\text{ave}} = 2.593$ and $(h_2)_{\text{ave}} = 2.566$. The theoretical $m = 0$ Fourier coefficient of Table 1 deviates from these values by only 0.06% and 0.99%, respectively. But the most apparent feature of Figs. 3(a) and 3(b) is the large noise level present in the data. The root-mean-square deviation of the data from the $0 \leq m \leq 4$ low-pass filtered data in Figs. 3(a) and 3(b) is 231% and 205% of the value of Δh_2 predicted from approximation (11). We were surprised by the magnitude of the noise, because in Section 2 we determined that the measurement uncertainty should be approximately only 25% of Δh_2. Although the inhomogeneity noise in Figs. 3(a) and 3(b) is substantial, it was not visually evident to us as we rotated the rod manually before taking the data. During manual rotation, ξ increased by a number of degrees per second, the fast fluctuations in the supernumerary spacing were smoothed, and only the slow sinusoidal variation of the supernumerary spacing was observed visually on a distant viewing screen.

After repeatedly testing the apparatus, we concluded that the high noise level in Figs. 3(a) and 3(b) does not arise from nonuniformities in the laser beam, optical interference with diffraction from the beam block, or nonuniformities in the polarizing filter. Each of these elements remained fixed during the experimental run. The noise is uncorrelated for $\Delta\xi = 2°$ and persisted when we examined a 10° rotation angle interval with $\Delta\xi = 0.083°$. Because the inhomogeneity noise is uncorrelated for $\Delta\xi = 2°$, the $0 \leq m \leq 4$ low-pass filtering of Figs. 3–6 largely removes it from the experimental data.

The noise appears to take the form of an expansion or contraction of the entire supernumerary pattern, i.e., a sudden rise or drop in $h_2(\xi)$ obtained from the first and second supernumerary maxima in Fig. 3(a) is almost always accompanied by a similar rise or drop in $h_2(\xi)$ obtained from the first and third supernumeraries in Fig. 3(b). Thus what we observe is not random noise superimposed on the data. Rather it appears to be the actual behavior of the entire supernumerary pattern. For these reasons we believe that the rapid fluctuations in $h_2(\xi)$ are due to perturbations in the shape of the wave front exiting the rod and that these perturbations are caused by the rod's small local refractive-index inhomogeneities. The reason this high noise level surprised us is that, because the rainbow supernumeraries were observed to be parallel straight lines and our measured $\theta_2{}^R(\xi)$ and $\theta_3{}^R(\xi)$ in Ref. 13 were free of noise, we presumed that $h_2(\xi)$ would be similarly noise free, except for the measurement uncertainty of approximation (20). What appears to be the case is that, because $h_2(\xi)$ was found in Ref. 6 to be such a delicate feature of the caustic, it is sensitive to any imperfection in the glass rod as well as to any uncertainty in the measured supernumerary angles.

When we now consider the Fourier-series decomposition of both the experimental data and the prediction of the ray-tracing–wave-front modeling calculation, the average inhomogeneity noise level in the experimental $3 \leq m \leq 6$ Fourier channels in Table 1 is $(e_m{}^2 + f_m{}^2)^{1/2} \approx 0.45$. Once we subtract this average noise level from the magnitude of the experimental $m = 2$ Fourier coefficient in Table 1,

assuming that the relative phase between the $m = 2$ coefficient and the inhomogeneity noise is random, the magnitude of the experimental $m = 2$ coefficient agrees with that of the theoretical $m = 2$ coefficient to within 8.8% and 1.2% for the data from the first and second and the first and third supernumeraries, respectively. The agreement between the $m = 0$ and $m = 2$ theoretical and experimental Fourier-series coefficients in Table 1 and the agreement between the low-pass filtered experimental data and the predictions of the ray-tracing–wave-front modeling calculation in Figs. 3(a) and 3(b) provide strong evidence that the approximation for the supernumerary spacing parameter in approximations (10)–(12) is accurate.

C. $p = 2$ Supernumeraries of the 2.44-mm-Radius Glass Rod

We first determined the refractive index and ellipticity of the 2.44-mm-radius rod using the same method as we used earlier for the 8.05-mm-radius rod.[13] We measured the position of the first supernumerary maximum of the $p = 2$ and $p = 3$ rainbows as a function of ξ, determined the rainbow angle using approximation (15), and performed the Fourier-series decomposition. We then determined the refractive index from the $m = 0$ Fourier coefficient of the $p = 2$ and $p = 3$ rainbows and the ellipticity from the $m = 2$ Fourier coefficient. We found that $n = 1.502 \pm 0.010$ and $\epsilon = 0.0054 \pm 0.0002$ produced the best fit to the combined $p = 3$ rainbow angle data. The average rod radius was measured with a micrometer.

With the CCD detector placed a distance $r = 132$ mm from the rod axis, we then determined $h_2(\xi)$ from the relative position of the first, second, third, and fourth supernumerary maxima and computed the Fourier-series decomposition of $h_2(\xi)$. Our results are shown in Table 1 and Fig. 4. The experimental data are the average of three separate measurements of $h_2(\xi)$ by use of the first and second, first and third, and first and fourth supernumeraries. This averaging procedure did not reduce the inhomogeneity noise, but greatly reduced the measurement uncertainty that was seen in Section 2 to be dangerously high. The root-mean-square deviation of the resulting data from the $0 \le m \le 4$ low-pass filtered data is 337% of the value of Δh_2 predicted by approximation (11). In Table 1 the $m = 0$ theoretical Fourier coefficient for $n = 1.502$ and $\epsilon = 0.0054$ contains the 3.6% near-zone correction for $r/a = 54.14$ and agrees to within 0.75% of the experimental value of $(h_2)_{\text{ave}}$. The average inhomogeneity noise level in the $3 \le m \le 6$ Fourier channels in Table 1 is $(e_m^2 + f_m^2)^{1/2} \approx 0.046$. Once we subtract the average noise level from the magnitude of the experimental $m = 2$ Fourier coefficient of Table 1 assuming a random phase difference, it agrees with the theoretical $m = 2$ coefficient to within 4.43%. The combined results of Fig. 4 and Table 1 again show good agreement between the experimental data and the ray-tracing–wave-front modeling prediction of approximations (10)–(12).

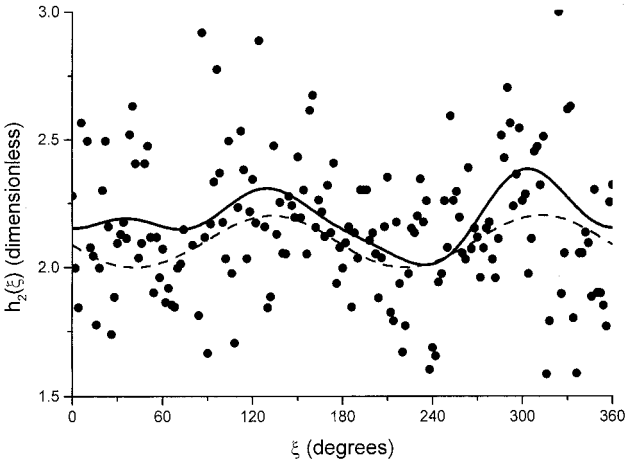

Fig. 4. Supernumerary spacing parameter of the $p = 2$ rainbow of a 2.44-mm-radius glass rod with refractive index $n = 1.502$ and eccentricity $\epsilon = 0.0054$ as a function of the rod's rotation angle. The solid circles are the experimental data that we obtained from averaging the results of the first and second, first and third, and first and fourth supernumerary maxima; the solid curve is the low-pass filtered experimental data; and the dashed curve is the prediction of the ray-tracing–wave-front modeling procedure of Ref. 6.

D. $p = 3$ Supernumeraries of the 8.05- and 2.44-mm-Radius Rods

We also measured the relative position of the first, second, and third supernumerary maxima of the $p = 3$ rainbow for our two glass rods. We then determined $h_3(\xi)$ using the $p = 3$ version of Eq. (18) and performed the Fourier-series decomposition of the experimental results:

$$h_3(\xi) = g_0 + \sum_{m=1}^{\infty} g_m \cos(m\xi) + \sum_{m=1}^{\infty} j_m \sin(m\xi). \quad (22)$$

The experimental data for the 8.05- and 2.44-mm-radius rods and the theoretical predictions of the ray-tracing–wave-front modeling calculations are shown in Table 2 and Figs. 5 and 6. The experimental data are the average of two separate measurements of

Table 2. Magnitude of the Coefficients in the Fourier-Series Decomposition of $h_3(\xi)$ for the 8.05- and 2.44-mm-Radius Glass Rods[a]

Fourier Coefficient	$a = 8.05$ mm		$a = 2.44$ mm	
	Experiment	Theory	Experiment	Theory
g_0	23.018	16.971	12.496	13.249
$(g_1^2 + j_1^2)^{1/2}$	1.107	0.000	0.582	0.0
$(g_2^2 + j_2^2)^{1/2}$	7.830	8.249	1.256	0.980
$(g_3^2 + j_3^2)^{1/2}$	5.728	0.000	1.514	0.0
$(g_4^2 + j_4^2)^{1/2}$	2.799	0.598	0.318	0.012
$(g_5^2 + j_5^2)^{1/2}$	2.810	0.000	0.476	0.0
$(g_6^2 + j_6^2)^{1/2}$	3.140	0.136	0.543	6×10^{-4}

[a]We obtained the experimental coefficients by averaging $h_3(\xi)$ obtained from the first and second and the first and third supernumerary maxima. The ray-tracing–wave-front modeling Fourier coefficients are for $n = 1.474$ and $\epsilon = -0.037$ and for $n = 1.511$ and $\epsilon = 0.0054$. The $m = 0$ theoretical coefficient was corrected for near-zone effects with $r/a = 42.35$ and $r/a = 54.14$.

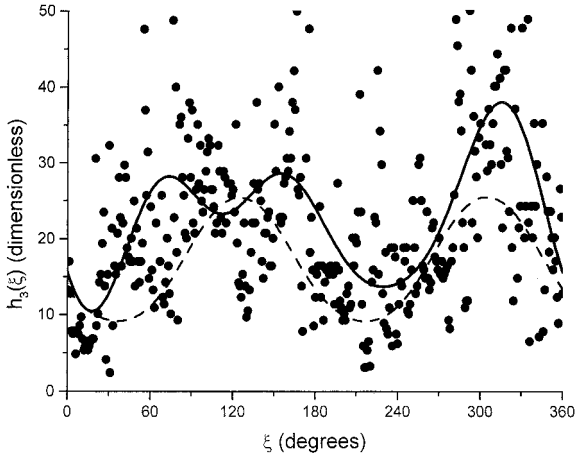

Fig. 5. Supernumerary spacing parameter of the $p = 3$ rainbow of a 8.05-mm-radius glass rod with refractive index $n = 1.474$ and eccentricity $\epsilon = -0.037$ as a function of the rod's rotation angle. The solid circles are the experimental data that we obtained from averaging the results of the first and second and the first and third supernumerary maxima, the solid curve is the low-pass filtered experimental data, and the dashed curve is the prediction of the ray-tracing–wave-front modeling procedure of Ref. 6.

$h_3(\xi)$ that we obtained using the first and second and the first and third supernumerary maxima. The theoretical $m = 0$ Fourier coefficient contains the 1.58% and 1.47% near-zone correction of Ref. 19 for the experimental r/a ratios for the two rods and differs from the experimental $m = 0$ coefficient by 35.6% and 5.7%, respectively. We do not know the reason for the large difference between the $m = 0$ coefficients for the 8.05-mm rod.

Because $h_3{}^c/h_2{}^c \approx 6$, the measurement uncertainty $\delta h_3/h_3{}^c$ in the $p = 3$ supernumerary data

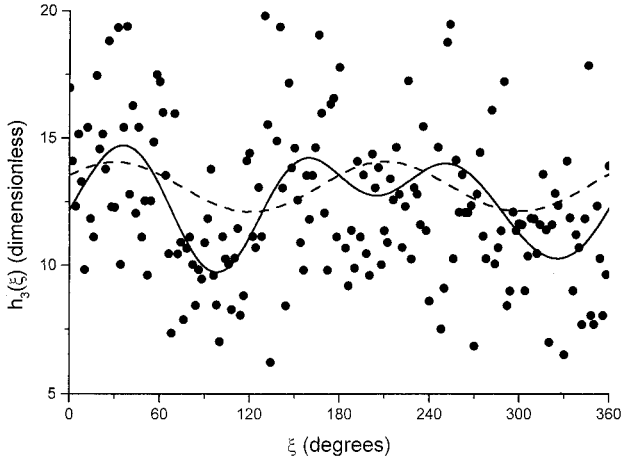

Fig. 6. Supernumerary spacing parameter of the $p = 3$ rainbow of a 2.44-mm-radius glass rod with refractive index $n = 1.502$ and eccentricity $\epsilon = 0.0054$ as a function of the rod's rotation angle. The solid circles are the experimental data that we obtained from averaging the results of the first and second and the first and third supernumerary maxima, the solid curve is the low-pass filtered experimental data, and the dashed curve is the prediction of the ray-tracing–wave-front modeling procedure of Ref. 6.

should be approximately $(1/6)^{1/3} \approx 0.55$ of that for $\delta h_2/h_2{}^c$. But as was the case for the $h_2(\xi)$ data in Figs. 3 and 4, the $h_3(\xi)$ data of Figs. 5 and 6 contain a large amount of inhomogeneity noise, with the root-mean-square deviation of the data from the $0 \leq m \leq 4$ low-pass filtered data for the 8.05- and 2.44-mm-radius rods being 147% and 350% of the value of the theoretical $m = 2$ Fourier coefficient, our estimate for Δh_3. The average inhomogeneity noise in the $m = 1, 4, 5, 6$ Fourier channels in Table 2 is $(g_m{}^2 + j_m{}^2)^{1/2} \approx 2.464$ and 0.480. When we subtract this noise from the experimental $m = 2$ Fourier coefficient assuming a random phase difference, the result agrees with the theoretical $m = 2$ Fourier coefficient to within 9.1% and 15.2%. This is an encouraging sign, again illustrating the basic correctness of the ray-tracing–wave-front modeling procedure of Ref. 6 as applied to $h_3(\xi)$.

In Ref. 13 we had found that the $p = 2$ rainbow angle was rather insensitive to a small amount of nonellipticity in the rod cross section, but there was a marked sensitivity of the $p = 3$ rainbow angle to rod nonellipticity. On the basis of this sensitivity of the $p = 3$ rainbow angle, we determined that, when the cross section of the 8.05-mm rod was modeled by two half-ellipses of differing eccentricities $\epsilon_1 = -0.050$ and $\epsilon_2 = -0.024$ smoothly joined together along the major axis, the prediction of the ray-tracing calculation fit the experimental $p = 2$ and $p = 3$ rainbow angles as a function of ξ rather well.

We also examined the effects of cross-sectional nonellipticity on the supernumerary spacing parameter using the ray-tracing–wave-front modeling procedure and a cross section of two half-ellipses. The prediction for $h_2(\xi)$ with $n = 1.474$, $\epsilon_1 = -0.050$, and $\epsilon_2 = -0.024$ remained approximately sinusoidal with the amplitude of oscillation increasing by approximately 12% from the elliptical cross-sectional case $n = 1.474$ and $\epsilon = -0.037$. Thus both $\theta_2{}^R(\xi)$ and $h_2(\xi)$ are relatively insensitive to a small amount of rod ellipticity. However, for $n = 1.474$, $\epsilon_1 = -0.050$, and $\epsilon_2 = -0.024$, the predicted oscillation in $h_3(\xi)$ exhibited larger deviations from a sinusoidal behavior with the amplitude of oscillation increasing by approximately 24% from the $n = 1.474$ and $\epsilon = -0.037$ elliptical cross-sectional case. As a result, a small amount of rod nonellipticity is likely to be a significant factor in the interpretation of the $h_3(\xi)$ data of Figs. 5 and 6. The fact that the double-hump behavior seen in Figs. 5 and 6 at $\xi \approx 120°$ and $\xi \approx 210°$ was not reproduced by the two half-ellipses model, whereas a similar double-hump structure in the $p = 3$ rainbow angle shown in Fig. 6 of Ref. 11 was reproduced by the two half-ellipses model, may signal that $h_3(\xi)$ is much more sensitive to the exact form of the nonellipticity than is $\theta_3{}^R(\xi)$. Until a better modeling procedure for the rod cross section is available, a detailed quantitative comparison between theory and the experimental results of Figs. 5 and 6 is premature.

4. Discussion

When an elliptical cross-sectional rod is illuminated at normal incidence by a plane wave and is rotated about its axis, the first-order rainbow undergoes a number of changes. When observed on a distant viewing screen, it is quite evident that the entire rainbow pattern moves back and forth. To see this, all one has to do is mark the rainbow position on the viewing screen for a particular rod orientation and then watch the rainbow move with respect to the mark as the rod is rotated. Similarly, the rainbow intensity variations are easily observable. But it requires more careful observation to realize that the supernumerary spacing is simultaneously expanding or contracting as well, because, for the 8.05-mm-radius rod, the amount of expansion and contraction is approximately only 21% for the $p = 2$ rainbow and approximately 34% for the $p = 3$ rainbow.

In rainbow refractometry,[20,21] the refractive index and size of a falling spherical liquid droplet can be determined when the features of its first-order rainbow are examined. After measuring the angular position of the first two supernumerary maxima $\theta_a^{\max}$ and $\theta_b^{\max}$, one can obtain the rainbow angle from Eq. (17), then the refractive index from Eqs. (3), then the supernumerary spacing parameter from Eq. (4), and finally the particle radius from Eqs. (1) and (18). If the falling droplet has an oblate spheroidal rather than a spherical shape because of flattening produced by air resistance, the value of n and a determined in this manner, assuming a spherical shape, will be in error.[22] Two experimental tests for asphericity have been proposed for rejecting rainbow refractometry measurements made on aspherical droplets.[23,24]

It appears that the size of the error in n and a caused by either droplet asphericity or uncertainty in the measured values of $\theta_a^{\max}$ and $\theta_b^{\max}$ has not been studied systematically. We derive these errors as follows. When we differentiate Eqs. (3), a change $\delta\theta_p^D$ in the p-rainbow angle produces a change dn in the refractive index of

$$dn = n(n^2 - 1)^{1/2}\delta\theta_p^D/[2(p^2 - n^2)^{1/2}]. \quad (23)$$

Similarly, when we differentiate Eq. (4), a change dn in the refractive index produces a change dh in the supernumerary spacing parameter of

$$dh = -n(p^2 - 1)^2(3p^2 - 2n^2 - 1)dn/[p^2(p^2 - n^2)^{1/2}(n^2 - 1)^{5/2}]; \quad (24)$$

and when we differentiate Eq. (18), a change dh in the supernumerary spacing parameter produces a fractional change da/a in the particle radius of

$$da/a = dh/(2h). \quad (25)$$

If the droplet being studied is spherical and the angular position of the first two supernumerary maxima of the $p = 2$ rainbow is measured with the precision $\pm\delta\theta_{ab}$ deg, the uncertainty in the rainbow angle is given by approximation (19). If the refractive index and the particle size are obtained with Eqs. (17), (3), (4), and (18) as described above, the uncertainty in n and a is

$$dn/n = (n^2 - 1)^{1/2}(\pi/180)\delta\theta_{ab}/[2(4 - n^2)^{1/2}], \quad (26)$$

$$da/a = n^2(11 - 2n^2)(\pi/180)\delta\theta_{ab}/[4(n^2 - 1)^{1/2}(4 - n^2)^{3/2}]. \quad (27)$$

On the other hand, if the $p = 2$ supernumerary maxima are measured with perfect accuracy but the droplet being studied is an oblate spheroid with eccentricity ϵ, the maximum uncertainty in the rainbow angle is given by $\Delta\theta_2^R$ in Eq. (9). The resulting maximum uncertainty in n and a becomes

$$dn/n = 32(n^2 - 1)^2\epsilon/(9n^4), \quad (28)$$

$$da/a = 16(11 - 2n^2)(n^2 - 1)\epsilon/[9n^2(4 - n^2)]. \quad (29)$$

In either case, we obtain

$$(da/a)/(dn/n) = n^2(11 - 2n^2)/[2(n^2 - 1)(4 - n^2)]. \quad (30)$$

As an example of these error estimates, consider a spherical water droplet with $n = 1.33$. For either type of error, Eq. (30) yields $(da/a)/(dn/n) = 3.8$, illustrating that the uncertainty in the determined particle size is substantially larger than the uncertainty in the determined refractive index. This is because of the sensitive dependence of h on n in Eq. (24). These results also underscore the principal theme of both this paper and Ref. 6, i.e., that the supernumerary spacing is a surprisingly sensitive and delicate feature of the rainbow.

This research was supported in part by the National Science Foundation under grant PHY-9987862 and by the National Aeronautics and Space Administration under grant NCC-3-521.

References

1. W. Möbius, "Zur Theorie des Regenbogens und ihrer experimentallen Prufung," Abh. Math.-Phys. Kl. Saechs. Ges. Wiss. **30,** 105–254 (1907–1909).
2. W. Möbius, "Zur Theorie des Regenbogens und ihrer experimentallen Prufung," Ann. Phys. (Leipzig) **33,** 1493–1558 (1910).
3. G. P. Können, "Appearance of supernumeraries of the secondary rainbow in rain showers," J. Opt. Soc. Am. A **4,** 810–816 (1987).
4. A. B. Fraser, "Why can the supernumerary bows be seen in a rain shower?" J. Opt. Soc. Am. **73,** 1626–1628 (1983), color plate 1.
5. A. B. Fraser, "Chasing rainbows," Weatherwise **36,** 280–287 (1983).
6. J. A. Lock, "Supernumerary spacing of rainbows produced by an elliptical-cross-section cylinder. I. Theory," Appl. Opt. **39,** 5040–5051 (2000).
7. H. C. van de Hulst, *Light Scattering by Small Particles* (Dover, New York, 1981), Sect. 13.23, pp. 243–246.
8. R. T. Wang and H. C. van de Hulst, "Rainbows: Mie computations and the Airy approximation," Appl. Opt. **30,** 106–117 (1991).
9. J. P. A. J. van Beeck, "Rainbow phenomena: development of a laser-based, non-intrusive technique for measuring droplet

size, temperature and velocity," Ph.D. dissertation (Eindhoven Technische Universiteit, Eindhoven, The Netherlands, 1997), p. 78.
10. M. Abramowitz and I. A. Stegun, eds., *Handbook of Mathematical Functions* (National Bureau of Standards, Washington D.C., 1964), Sect. 10.4, pp. 446–447, 478.
11. J. D. Walker, "Multiple rainbows from single drops of water and other liquids," Am. J. Phys. **44,** 421–433 (1976).
12. M. V. Berry, "Waves and Thom's theorem," Adv. Phys. **25,** 1–26 (1976).
13. C. L. Adler, J. A. Lock, and B. R. Stone, "Rainbow scattering by a cylinder with a nearly elliptical cross section," Appl. Opt. **37,** 1540–1550 (1998).
14. C. L. Adler, J. A. Lock, B. R. Stone, and C. J. Garcia, "High-order interior caustics produced in scattering of a diagonally incident plane wave by a circular cylinder," J. Opt. Soc. Am. A **14,** 1305–1315 (1997).
15. J. A. Lock and C. L. Adler, "Debye-series analysis of the first-order rainbow produced in scattering of a diagonally incident plane wave by a circular cylinder," J. Opt. Soc. Am. A **14,** 1316–1328 (1997).
16. J. A. Lock, C. L. Adler, B. R. Stone, and P. D. Zajak, "Amplification of high-order rainbows of a cylinder with an elliptical cross section," Appl. Opt. **37,** 1527–1533 (1998).
17. V. Khare and H. M. Nussenzveig, "Theory of the rainbow," Phys. Rev. Lett. **33,** 976–980 (1974).
18. Ferguson's Cut Glass Originals, 4292 Pearl Road, Cleveland, Ohio 44109.
19. J. A. Lock, C. L. Adler, and E. A. Hovenac, "Exterior caustics produced in scattering of a diagonally incident plane wave by a circular cylinder: semiclassical scattering theory analysis," J. Opt. Soc. Am. A **17,** 1846–1856 (2000).
20. N. Roth, K. Anders, and A. Frohn, "Refractive-index measurements for the correction of particle sizing methods," Appl. Opt. **30,** 4960–4965 (1991).
21. J. P. A. J. van Beeck and M. L. Riethmuller, "Nonintrusive measurements of temperature and size of single falling raindrops," Appl. Opt. **34,** 1633–1639 (1995).
22. P. L. Marston, "Rainbow phenomena and the detection of nonsphericity in drops," Appl. Opt. **19,** 680–685 (1980).
23. J. P. A. J. van Beeck and M. L. Riethmuller, "Rainbow phenomena applied to the measurement of droplet size and velocity and to the detection of nonsphericity," Appl. Opt. **35,** 2259–2266 (1996).
24. H. Lohner, P. Lehmann, and K. Bauckhage, "Detection based on rainbow refractometry of droplet sphericity in liquid–liquid systems," Appl. Opt. **38,** 1127–1132 (1999).